

Metal–Organic Frameworks

Selective Sensing of Fe³⁺ and Al³⁺ Ions and Detection of 2,4,6-Trinitrophenol by a Water-Stable Terbium-Based Metal–Organic FrameworkLi-Hui Cao,^[a] Fang Shi,^[a] Wen-Min Zhang,^[a] Shuang-Quan Zang,^{*,[a]} and Thomas C. W. Mak^[a, b]

Abstract: A water-stable luminescent terbium-based metal–organic framework (MOF), {[Tb(L₁)_{1.5}(H₂O)]·3H₂O}_n (Tb-MOF), with rod-shaped secondary building units (SBUs) and honeycomb-type tubular channels has been synthesized and structurally characterized by single-crystal X-ray diffraction. The high green emission intensity and the microporous nature of the Tb-MOF indicate that it can potentially be used as a lu-

minescent sensor. In this work, we show that Tb-MOF can selectively sense Fe³⁺ and Al³⁺ ions from mixed metal ions in water through different detection mechanisms. In addition, it also exhibits high sensitivity for 2,4,6-trinitrophenol (TNP) in the presence of other nitro aromatic compounds in aqueous solution by luminescence quenching experiments.

Introduction

Porous metal–organic frameworks (MOFs) are an important class of multifunctional materials used in many practical applications,^[1,2] including gas storage and separation, heterogeneous catalysis, and guest species recognition and adsorption, etc. The tunable structures and properties of porous MOFs provide an important advantage to chemosensory and adsorptive materials. Among the successful production of functional porous MOFs, lanthanide metal–organic frameworks (Ln-MOFs) are fascinating because of their versatile coordination geometry, high stability, and unique luminescent and magnetic properties.^[3] Owing to their high color purity and the long lifetimes of their excited states, the intriguing luminescence of lanthanide ions has potential applications in optical communications as well as fluorescent probes.^[4] In the past few years, fluorescent probes based on luminescent Ln-MOFs have been widely investigated for the selective detection of metal ions or small organic molecules as a result of their ability to provide a simple, selective, and sensitive detection method.^[5]

Iron and aluminium are ubiquitous metals in our living environment, and their cations also play crucial roles in the human body and other biological tissues. The Fe³⁺ ion influences electron transfer and oxygen metabolism processes in DNA and

RNA synthesis. Both excess and deficiency from the normal permissible limit can induce serious disorders.^[6] On the other hand, the Al³⁺ ion is not a necessary microelement for the human body, and its concentration level has a direct impact on human health. Because of the frequent use of aluminum cookware, the risk of the absorption of Al³⁺ ions by the human body is increasing. Many diseases can be caused by iron poisoning or aluminum toxicity, such as microcytic hypochromic anemia, bone softening, encephalopathy, myopathy, and Alzheimer's disease, etc.^[7] Therefore, the selective detection of Fe³⁺ and Al³⁺ is very important for human health. Recently, many excellent studies, based on Ln-MOFs or Ln@MOFs that can selectively sense metal ions such as Fe³⁺, Cu²⁺ ions or organic molecules such as acetone, have been reported by our group^[8] and other groups.^[9]

Nitro aromatic compounds such as nitrobenzene (NB), 1,3-dinitrobenzene (1,3-DNB), 1,4-dinitrobenzene (1,4-DNB), 2-nitrotoluene (2-NT), 2,4-dinitrotoluene (2,4-DNT), 2,6-dinitrotoluene (2,6-DNT), 2,4,6-trinitrotoluene (TNT), and 2,4,6-trinitrophenol (TNP) are the primary components of industrial explosives, environmentally deleterious substances, and many unexploded land mines.^[10] Hence, for the sake of security, military applications, and environmental concerns, the reliable and convenient detection of explosives has become a pressing issue.^[11,12] Owing to the unique selectivity, sensitivity, short response time, and convenient visual detection, fluorescence-based detection of nitro aromatic explosives by using luminescent metal–organic frameworks has attracted much attention since the first work reported in 2009.^[13] Of all the nitro aromatic explosives, TNP is one of the most powerful explosives, and is commonly used in dyes, fireworks, and pesticides.^[14] However, owing to their strong electron affinities, it is still a challenge to selectively detect TNP in the presence of other nitro aromatic explosives.^[15] Although some Ln-MOFs have been employed for explosive detection, only a few reports of Ln-MOF or

[a] L.-H. Cao, F. Shi, W.-M. Zhang, Prof. S.-Q. Zang, Prof. T. C. W. Mak
College of Chemistry and Molecular Engineering
Zhengzhou University
Zhengzhou (P. R. China)
Fax: (+86) 371-6778-0136
E-mail: zangsqz@zzu.edu.cn

[b] Prof. T. C. W. Mak
Department of Chemistry and Center of Novel Functional Molecules
The Chinese University of Hong Kong
Shatin, New Territories, Hong Kong SAR (P. R. China)

Supporting information for this article is available on the WWW under <http://dx.doi.org/10.1002/chem.201501162>.

Ln@MOFs based probes can selectively detect TNP in the presence of other nitro aromatic compounds in aqueous media.^[16]

Because of the oxophilic nature of lanthanide ions, the use of terephthalic acid and its derivatives to act as chromophoric ligands is one of the most common and efficient methods to construct novel lanthanide-containing porous MOFs with interesting structures and high luminescence quantum yields in previous reports.^[11c,17] Herein, we reported a water-stable terbium-based metal–organic framework, $\{[\text{Tb}(\text{L}_1)_{1.5}(\text{H}_2\text{O})]\cdot 3\text{H}_2\text{O}\}_n$ (Tb-MOF), which is based on a derivative of terephthalic acid, with strong luminescence intensity and that possesses 1D rod-shaped $[\text{Tb}(\text{CO}_2)_3]_n$ building units and honeycomb-type tubular channels. Tb-MOF can rapidly sense Fe^{3+} and Al^{3+} ions from mixed metal ions through different detection mechanisms. Tb-MOF also exhibits high sensitivity for 2,4,6-trinitrophenol (TNP) in the presence of other nitro aromatic compounds in aqueous solution through luminescence quenching experiments.

Results and Discussion

Single-crystal X-ray diffraction (XRD) analysis^[18] revealed that Tb-MOF crystallizes in the trigonal space group $R\bar{3}$. As shown in Figure S1 in the Supporting Information, the fundamental building unit of Tb-MOF contains one Tb^{3+} ion, one and a half L_1^{2-} ligands, and one coordinated water molecule. The three carboxylate groups of the one and a half L_1^{2-} ligands have two different coordination modes: one carboxylate bridges two Tb^{3+} ions in a bidentate fashion, whereas the other two carboxylate groups chelate and bridge two Tb^{3+} centers (Figure S2 in the Supporting Information). The Tb^{3+} center is coordinated to eight carboxyl oxygen atoms from six L_1^{2-} ligands and one water molecule. The nine-coordinate Tb^{3+} ions are further bridged by oxygen atoms from the carboxylate groups to form infinite 1D rod-shaped $[\text{Tb}(\text{CO}_2)_3]_n$ secondary building units (SBUs) running along the c axis (Figure 1b). This represents an efficient strategy to construct robust porous MOFs by utilizing rod-shaped SBUs.^[19] Each Tb–carboxylate infinite SBU is connected to three other chains through L_1^{2-} linkers to generate an interesting 3D coordination network with honeycomb-type channels propagated along the c axis (Figure 1c). The diameter of the 1D channel is 9.735 Å (opposite C18 to C18 distance), in which the vacancies are filled with solvent molecules. PLATON^[20] calculations indicate that the vacant space in Tb-MOF is about 25.1% of the crystal volume (2539.2 Å³ of the 10114.1 Å³ unit-cell volume) when the guests and coordinated water molecules are removed. In addition, if each metal center can be considered as a six-connected node and the two kinds of ligands as four-connected spacers, the whole architecture is a 4,6-connected **stp** net with a Schläfli symbol of $\{4^4\cdot 6^2\}_3\{4^9\cdot 6^6\}_2$ calculated with TOPOS^[21] (Figure 1d).

Luminescence properties of Tb-MOF

The room-temperature solid-state photoluminescent excitation and emission spectra of the Tb-MOF are shown in Figure 2. Tb-MOF shows emission peaks at 488, 541, 585, and 619 nm arising from the $^5\text{D}_4 \rightarrow ^7\text{F}_J$ ($J=6, 5, 4,$ and 3) transitions of the Tb^{3+}

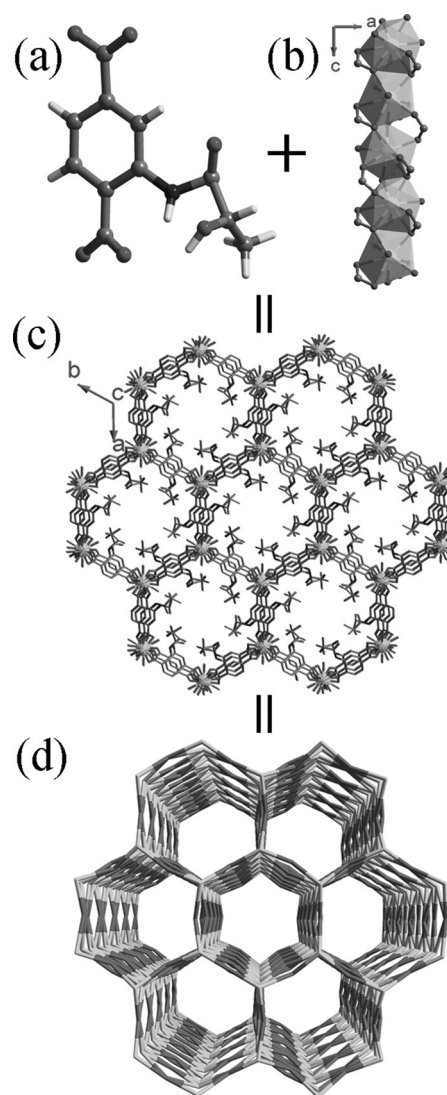


Figure 1. (a) Structure of organic ligand L_1^{2-} . (b) The infinite 1D rod-shaped $[\text{Tb}(\text{CO}_2)_3]_n$ SBUs running along the c axis. (c) 3D coordination framework with honeycomb-type channels. (d) Schematic representation of the 4,6-connected **stp** network with a Schläfli symbol of $\{4^4\cdot 6^2\}_3\{4^9\cdot 6^6\}_2$.

ion upon excitation at 329 nm. Of these characteristic lines of the Tb^{3+} ion, the green luminescence peak at 541 nm is the most prominent. In addition, it is worth noting that the ligand-centered broad emission is not observed in the solid-state photoluminescent emission spectrum of Tb-MOF, indicating the occurrence of the “antenna effect”: L_1^{2-} moieties adsorb the energy and, by vibronic coupling between L_1^{2-} and Tb^{3+} , transfer energy to Tb^{3+} , leading to the strong luminescence of Tb^{3+} . The excitation spectrum collected at the wavelength of 541 nm displays a dominating broad band in the range of 250–400 nm, originating from the absorption of the L_1^{2-} ligand (Figure S4 in the Supporting Information), providing further evidence for the “antenna effect”.

Before studying the properties of Tb-MOF, we first examined the water stability. Tb-MOF crystals were immersed in water for 45 days at room temperature. Powder XRD patterns of the as-synthesized and water-treated samples completely overlap

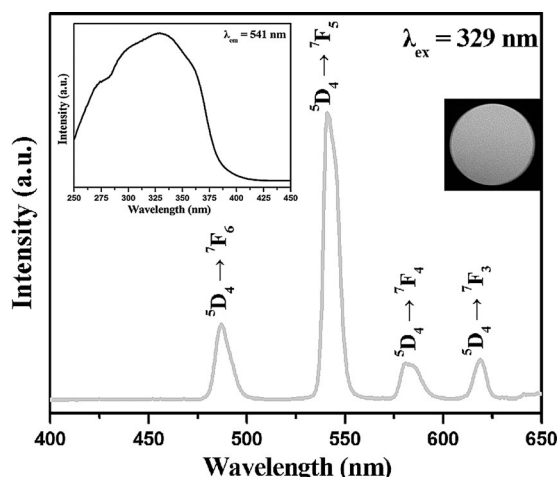


Figure 2. Emission spectrum of Tb-MOF in the solid state at room temperature. The insets are the corresponding excitation spectrum and luminescence picture under UV-light irradiation at 365 nm.

that of the simulated pattern from single-crystal analysis (Figure S5 in the Supporting Information), indicating the retention of the framework of Tb-MOF after water treatment. The good stability of the Tb-MOF emission in the aqueous environment can probably be ascribed to the sufficient protection of Tb^{3+} provided by the MOF scaffold. This compatibility with aqueous environments makes Tb-MOF well suited for generating new fluorescence probes for the aqueous environmental systems.

Sensing of metal ions

To examine the potential of Tb-MOF for sensing of metal ions, the as-synthesized samples were ground and immersed in aqueous solutions containing different metal ions (Li^+ , Na^+ , K^+ , Mg^{2+} , Ca^{2+} , Sr^{2+} , Ba^{2+} , Al^{3+} , Fe^{3+} , Fe^{2+} , Co^{2+} , Ni^{2+} , Cu^{2+} , Zn^{2+} , Cd^{2+} , Ag^+ , and Pb^{2+}) to form a metal-ion-incorporated MOF suspension. The luminescent spectra and corresponding excitation spectra were recorded and are compared in Figure 3 as well as Figure S6 in the Supporting Information. The emission spectra show that the various metal ions display markedly different effects on the luminescence of the Tb^{3+} ion. For example, the effect on the luminescence intensity of Tb-MOF at 541 nm is negligible when Li^+ , Na^+ , K^+ , Mg^{2+} , Ca^{2+} , Sr^{2+} , Ba^{2+} , Fe^{2+} , Co^{2+} , Ni^{2+} , Zn^{2+} , Cd^{2+} , Ag^+ , or Pb^{2+} are involved, whereas Al^{3+} , Cu^{2+} , and Fe^{3+} exhibit varying extents of quenching on the luminescence of Tb^{3+} , and their emission spectra are different and easily distinguished: Cu^{2+} has a quenching effect on luminescence intensity to a certain degree; Al^{3+} can quench the emission of Tb^{3+} , whereas the emission of the ligand has been enhanced to a large extent, giving rise to a bright blue light (Figure 3). However, unlike Cu^{2+} or Al^{3+} , Fe^{3+} can completely quench the emission of Tb-MOF. As a result, its emission color under UV light is dark. The remarkable enhancing and quenching effects can be further confirmed by the photographs of the Al^{3+} @Tb-MOF and Fe^{3+} @Tb-MOF suspensions under UV-light irradiation (the inset pictures in Figure 3). These results indicate that Tb-MOF can selec-

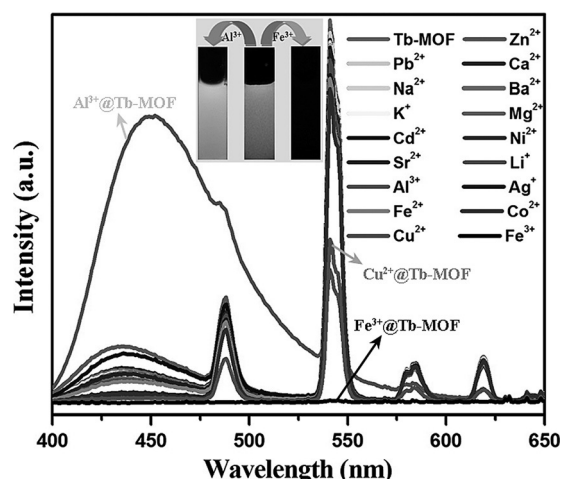


Figure 3. Fluorescence spectra of Tb-MOF (10 mg) in aqueous solutions of various metal cations (3 mL, 10 mM). The inset is the corresponding photographs under UV-light irradiation at 365 nm.

tively sense Fe^{3+} through fluorescence quenching of the characteristic lines of the Tb^{3+} ion and selectively detect Al^{3+} through fluorescence enhancement of the ligand, which is quite rare in the previous reports on luminescent MOFs.

To validate the high selectivity of Tb-MOF for detection of Fe^{3+} and Al^{3+} , competitive experiments of coexisting ions were performed under the same conditions. Upon the introduction of Fe^{3+} to the mixture of Tb-MOF and other metal cations, the fluorescence is significantly quenched (Figure S7a in the Supporting Information). Similarly, when introducing Al^{3+} to the mixture of Tb-MOF and other metal cations except Fe^{3+} , the fluorescence of the ligand is significantly enhanced (Figure S7b in the Supporting Information). This reveals that the interference from conventional metal cations can be neglected; only Cu^{2+} might interfere with the detection of Fe^{3+} to a small degree, further confirming the selectivity of Tb-MOF for Fe^{3+} and Al^{3+} detection and the potential of Tb-MOF for practical use.

To better understand the fluorescence response of Tb-MOF to Fe^{3+} and Al^{3+} , concentration-dependent luminescence measurements were also carried out. The as-synthesized Tb-MOF solid samples were ground and immersed in different concentrations of Fe^{3+} or Al^{3+} , and then their luminescence spectra were recorded. As demonstrated in Figure 4, the emission intensity of the Tb-MOF suspension was quenched steadily with increasing Fe^{3+} concentration from 0–10 mM and enhanced accordingly with increasing Al^{3+} concentration from 0–100 mM. As shown in Figure 4b for the Al^{3+} loaded sample, the luminescence intensity of Tb^{3+} decreased slowly and the emission of the ligand increased gradually with an increase in the concentration of Al^{3+} . When the concentration reaches 10 mM, the quenching effect on the luminescence of Tb^{3+} is clear. When the concentration reaches 100 mM, the luminescence of Tb^{3+} is nearly completely quenched and only the emission of the ligand can be observed. As a result, under UV-light irradiation at 365 nm, with an increase in Al^{3+} , the colors of the Al^{3+} -loaded samples change from green to bright blue

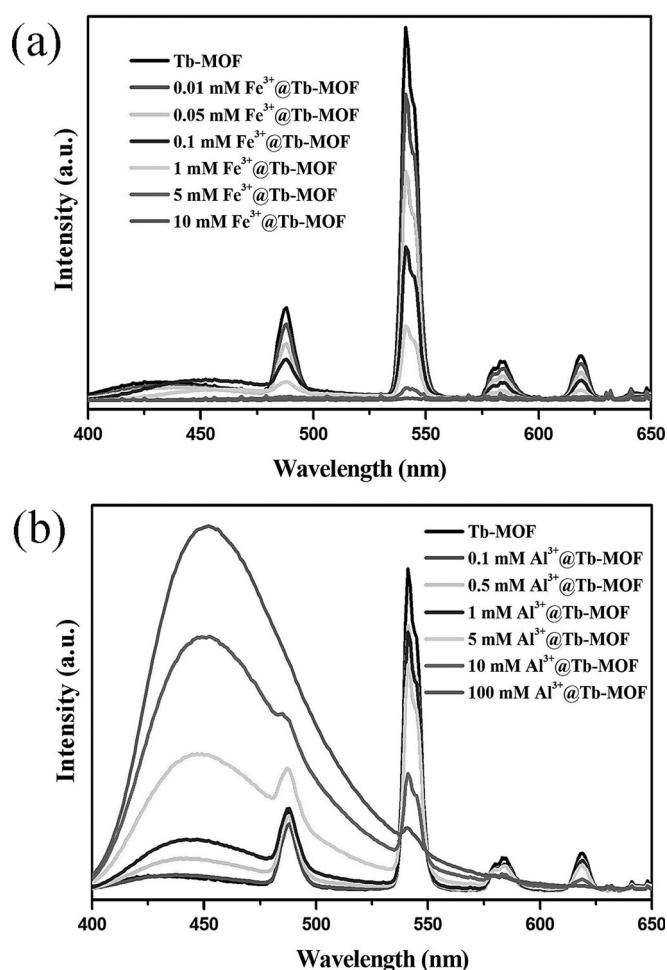


Figure 4. Emission spectra of Tb-MOF in aqueous solutions of various concentrations of Fe^{3+} (a) and Al^{3+} (b) under excitation at 329 nm.

(Figure S8 in the Supporting Information). Simultaneously, we discovered that the framework of the Tb-MOF dissolved gradually in water and that the solution was completely clear when the Al^{3+} concentration reached 0.1 mol L^{-1} . Reversible experiments were carried out, but unfortunately, the sensitivity of Tb-MOF for Fe^{3+} and Al^{3+} was not reversible (Figures S16 and S17 in the Supporting Information), which limited its recycle use.

Also, it should be noted that the addition of Cu^{2+} can cause partial luminescence intensity quenching of Tb-MOF, which may interfere with the detection of Fe^{3+} . So the concentration-dependent luminescence measurement of Cu^{2+} was carried out (Figure S9 in the Supporting Information). The results show that the quenching efficiency of Cu^{2+} is only half that of Fe^{3+} when the concentration is 10 mM. According to the corresponding photographs under UV-light irradiation at 365 nm, we also find that this small interference does not affect the detection of Fe^{3+} (insert pictures in Figure S9).

According to previous reports, the quenching effect on luminescence MOFs by metal cations may be attributed to the following factors:^[3c, 5f, 9a, 22–23] (a) interactions between metal cations and organic ligands; (b) collapse of the crystal structure

by the metal cations; (c) cation exchange between the central cations of the frameworks and the targeted cations. Powder XRD pattern studies of Tb-MOF and concentration-dependent Fe^{3+} @Tb-MOF (Figure S10 in the Supporting Information) disclosed that the crystalline structure of Tb-MOF was retained in the Fe^{3+} cation exchange process.

To further understand the process of cation exchange, we choose the concentration of 0.1 mol L^{-1} Fe^{3+} in aqueous solution for the next time-dependent experiments. The ground powder samples of Tb-MOF were introduced into the Fe^{3+} solution for different amounts of time (10 min, 30 min, 1 h, 2 h, 5 h, 24 h) to obtain the time-dependent Fe^{3+} @Tb-MOF samples, and then filtered and washed with fresh distilled water several times until the filtrate was completely colorless; this ensured that any metal cations physically adsorbed on the surface of the crystals had been washed off. Next, these time-dependent Fe^{3+} @Tb-MOF samples were dried in air. Then, we analyzed the time-dependent inductively coupled plasma spectroscopy (ICP) of solid samples of Fe^{3+} @Tb-MOF as well as the ICP of their filtrate after “ion exchanging”. Time-dependent ICP results (Table S3 in the Supporting Information) showed that the Tb^{3+} content of the filtrate after “ Fe^{3+} exchange” continues to increase and the Fe^{3+} concentration was decreased. Conversely, in the solid-state Fe^{3+} @Tb-MOF, the Fe^{3+} content continually increased and the Tb^{3+} content decreased with increasing immersion time. In addition, the luminescence intensity decreased gradually with increasing concentrations of the metal cations (Figure 4a). Combining these observations with the above experimental results, we proposed that some of the Tb^{3+} in the framework is substituted by Fe^{3+} and is dissolved in the Fe^{3+} aqueous solution, which reduces the energy transfer efficiency from the ligands to Tb^{3+} ions, thus leading to the quenching effect.

As shown in Figure S11 in the Supporting Information, when Al^{3+} was added to an aqueous solution of L_1^{2-} , the emission intensity of L_1^{2-} increased significantly. However, Tb^{3+} decreased the emission intensity of L_1^{2-} but the characteristic emission of Tb^{3+} increased, owing to the antenna effect. When both Al^{3+} and Tb^{3+} were added into the aqueous solution of L_1^{2-} , the characteristic emission intensity of Tb^{3+} was enhanced by the same amount as when only Tb^{3+} was added, and the emission intensity of the ligand was reduced, but less so than with Tb^{3+} alone. So, when Al^{3+} was added to the suspension of Tb-MOF, the mixture turned clear gradually, while at the same time, the emission intensity of L_1^{2-} increased and the characteristic emission intensity of Tb^{3+} decreased when Al^{3+} reached a certain concentration. The emission spectrum was similar to that of both Al^{3+} and Tb^{3+} being added to the aqueous solution of L_1^{2-} . The results showed that Al^{3+} can collapse the crystal structure of Tb-MOF to Tb^{3+} and L_1^{2-} , which were then dissolved in the aqueous solution.

Sensing of nitro explosives

To trace the ability of Tb-MOF to sense explosives, changes in the fluorescence intensity of Tb-MOF dispersed in water on addition of different nitro aromatic compounds, including TNT,

NB, 1,3-DNB, 1,4-DNB, 2-NT, 2,4-DNT, 2,6-DNT, and TNP in aqueous solutions (1 mM), were investigated (Figure S12 in the Supporting Information). The luminescence intensity of Tb-MOF at 541 nm is negligibly influenced by aqueous solutions of TNT, NB, 1,3-DNB, 1,4-DNB, 2-NT, 2,4-DNT, and 2,6-DNT, whereas very high levels of fluorescence quenching were observed in TNP aqueous solution. The visible yellow-green emission of Tb-MOF under UV light vanished upon the addition of the TNP solution, which quenched nearly 93% of the initial fluorescence intensity (Figure 5).

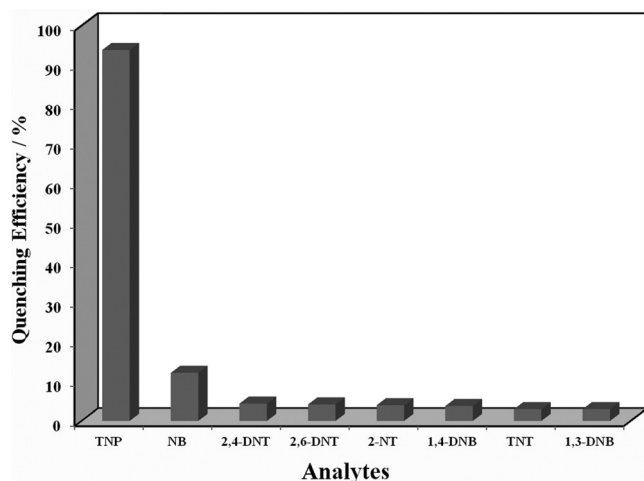


Figure 5. Quenching efficiency of Tb-MOF for different nitro analytes.

To explore the potential applications of Tb-MOF in the detection of TNP, fluorescence-quenching titrations were performed by gradual addition of TNP (10 mM in aqueous solution) to a dispersion of ground Tb-MOF in water. Very high levels of fluorescence quenching were observed upon incremental addition of TNP (Figure 6). In contrast, all of the other nitro analytes had a minor effect on the fluorescence intensity of Tb-MOF (Figure 5). This clearly indicates that Tb-MOF has high selectivity towards TNP over other nitro analytes. In addition, reversible experiments were performed, but TNP adsorption was also found to be irreversible on adding excess Tb^{3+} (Figure S18 in the Supporting Information), which limited its recycle use.

Encouraged by these results, the selectivity of Tb-MOF towards TNP in the presence of other nitro aromatic explosives was investigated under the same conditions. Upon the introduction of TNP to the mixture of Tb-MOF and other nitro aromatics, the fluorescence is quenched promptly (Figure S13 in the Supporting Information). The results indicate that the interference from conventional nitro aromatic explosives can be neglected, further confirming the high selectivity of Tb-MOF for TNP detection and the potential of Tb-MOF for practical use.

These results demonstrate that Tb-MOF has high selectivity for TNP compared with other nitro aromatics. Further, the fluorescence quenching efficiency was analyzed by using the Stern–Volmer (SV) equation (Figure 7), $I_0/I = K_{sv}[Q] + 1$, where, I_0 is the initial fluorescence intensity without any analyte, I is the

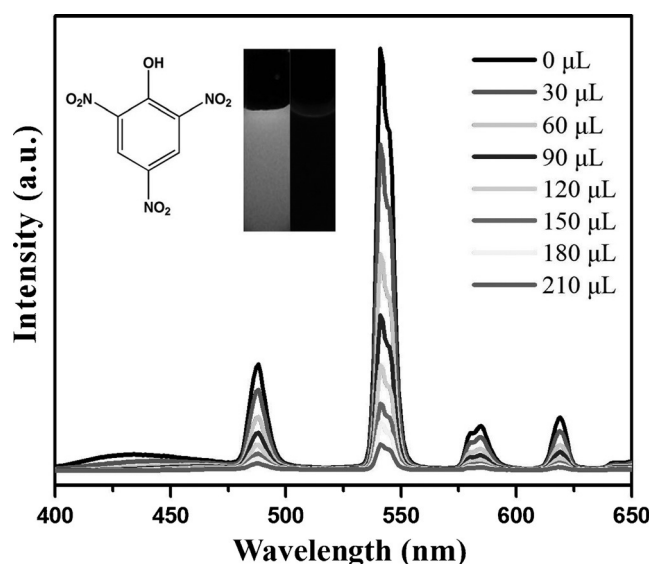


Figure 6. Emission spectra of Tb-MOF (10 mg) dispersed in water (3 mL) upon incremental addition of TNP solution (10 mM) in water. Inset: Photographs showing the original and the quenched fluorescence upon addition of TNP.

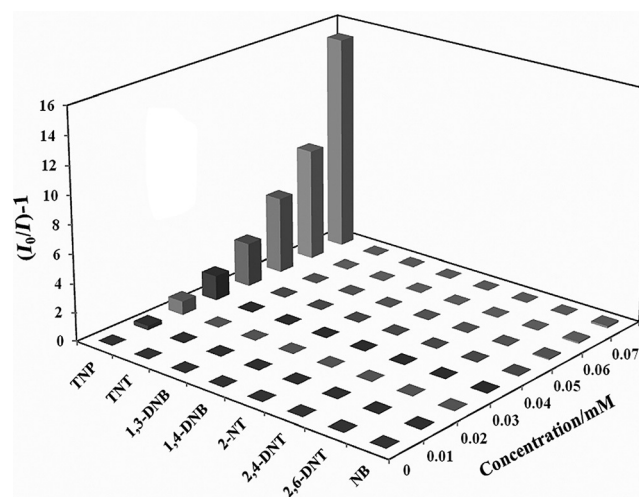


Figure 7. Stern–Volmer plot of various nitro analytes in water.

fluorescence intensity in the presence of the respective analyte, K_{sv} is the quenching constant, and $[Q]$ is the concentration of the analyte. As shown in Figure S14 in the Supporting Information, the SV plot for TNP was nearly linear at low concentrations and subsequently deviated from linearity, bending upwards at higher concentrations. The nonlinear nature of the SV plot of TNP can be attributed to self-absorption, a combination of static and dynamic quenching, or an energy-transfer process between TNP and the MOF.^[19a,24] The quenching constant (K_{sv}) for TNP was found to be $7.47 \times 10^4 \text{ M}^{-1}$, as verified by linear fitting of the SV plot at a low concentration range (0–0.04 mM, Figure S14).^[15a,25] Results indicate that strong interactions occur between TNP and the host framework.

Further studies of the UV/Vis absorption spectra of the nitro aromatic explosives show that the substituents on the aromat-

ic moieties can cause a different amount of red-shift of the $\pi \rightarrow \pi^*$ transitions. Under excitation at 329 nm, TNP has a higher absorbance and ϵ (molar extinction efficient) in comparison to the other analytes (Figure S15 in the Supporting Information), which can lead to lower absorption of the linker L_1^{2-} moieties. This implies that TNP the stronger quenching effect on the fluorescence intensity of Tb-MOF originates from the energy-transfer process between the ligands and metal centers. According to the above results, we can speculate the possible sensing mechanism for TNP explosive: The luminescence quenching of Tb-MOF by TNP is attributed to competition between the absorption of the light source energy and the electronic interaction between TNP and L_1^{2-} moieties.^[11c] TNP absorbs the excitation energy and decreases the light adsorbed by the L_1^{2-} moieties, so that the probability of energy transfer from L_1^{2-} to Tb^{3+} is reduced and subsequently the characteristic luminescence of Tb^{3+} is quenched. The SV plot, which deviates from linearity at high concentrations, also demonstrates the presence of both static and dynamic quenching mechanisms.

Conclusion

A honeycomb-type luminescent terbium-based metal-organic framework (Tb-MOF) was synthesized and characterized. Tb-MOF is highly selective and sensitive towards Fe^{3+} and Al^{3+} ions through different detection mechanisms. Most importantly, the selectivity for Fe^{3+} and Al^{3+} ions is not subject to interference by other mixed metal ions. In addition, Tb-MOF also shows highly selective and sensitive detection of TNP in aqueous media, even in the presence of other nitro aromatic compounds. The occurrence of both electron and energy-transfer processes, in addition to electrostatic interaction between the MOF and TNP, contribute to the selective fluorescence quenching. This work demonstrates the potential application of a fluorescent Tb-MOF as a multiresponsive probe for detection of explosives in the aqueous phase. The present results may provide a facile route to design and synthesize functional porous MOFs with applications in fluorescent sensors.

Experimental Section

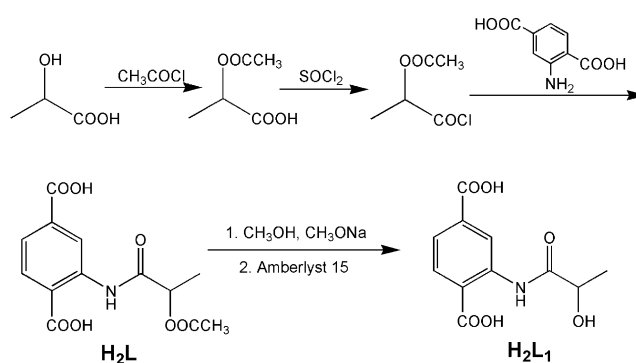
Materials and physical measurements

All the starting reagents and solvents employed in the present work were of analytical grade as obtained from commercial sources and used without further purification. 1H NMR spectra were recorded with a Bruker-400 spectrometer and the chemical shifts were reported in ppm using tetramethylsilane (TMS) as the internal standard. Elemental analysis for C, H, and N were performed on a PerkinElmer 240 elemental analyzer. The FTIR spectra were recorded from KBr pellets in the range 4000–400 cm^{-1} on a Nicolet NEXUS 470-FTIR spectrometer. Thermogravimetric analysis (TGA) was performed on an SDT 2960 thermal analyzer, under air, from room temperature to 800 °C with a heating rate of 20 °C min^{-1} . Powder X-ray diffraction data were collected on a Rigaku D/Max-2500PC diffractometer with $Cu_{K\alpha}$ radiation ($\lambda = 1.5406 \text{ \AA}$) over the 2θ range of 5–50° with a scan speed of 5°/min at room tempera-

ture. Luminescence spectra for the solid and suspension samples were recorded on a Hitachi 850 fluorescence spectrophotometer. Inductively coupled plasma spectroscopy (ICP) was performed on a Thermo ICAP 6500 DUO spectrometer. UV/Vis absorption spectra were measured with a TU-1901 double-beam UV/Vis spectrophotometer.

Preparation of 2-(2-Acetoxy-propionylamino)-terephthalic acid (H_2L) and 2-(2-Hydroxy-propionylamino)-terephthalic acid (H_2L_1)

The H_2L ligand was prepared by reaction of 2-acetoxypropionyl chloride with 2-amino-terephthalic acid (Scheme 1). 2-Acetoxypropionyl chloride was synthesized according to the literature procedure.^[26] 2-Acetoxypropionyl chloride (6.30 mL, 49.5 mmol) was added dropwise to a solution of 2-amino-terephthalic acid (3 g, 16.5 mmol) in *N,N'*-dimethylacetamide (DMAc) (20 mL). The resulting mixture was stirred at about 50 °C for 5.5 h. Water (80 mL) was added to the reaction mixture at room temperature, after which the suspension formed was cooled to a temperature between 0 °C and 5 °C and stirred for 30 min at this temperature. The suspension was filtered and the solid was washed with distilled water. The product was dried in a vacuum oven at 60 °C to yield 2-(2-acetoxypropionylamino)-terephthalic acid (3.93 g, 13.3 mmol, 80.6%). Elemental analysis calcd (%) for $C_{13}H_{13}O_7N$ (295.24): C 52.88, H 4.44, N 4.74; found: C 53.21, H 4.09, N 4.91; 1H NMR (300 MHz, DMSO): $\delta = 9.12$ (s, 1H), 8.09 (d, 1H), 7.70 (d, 1H), 5.16 (m, 1H), 2.20 (d, 3H), 1.46 ppm (d, 3H); IR (KBr): 2995 (w), 1753 (m), 1691 (vs), 1577 (s), 1539 (s), 1417 (m), 1275 (s), 1219 (vs), 1080 (m), 914 (m), 775 (m), 536 cm^{-1} (w).



Scheme 1. The synthesis of ligands H_2L and H_2L_1 .

H_2L (3.0 g, 10.0 mmol) was dissolved in methanol (60 mL) with a stoichiometric amount of CH_3ONa and the mixture was stirred for 20 h at room temperature. Subsequently, Amberlyst 15 (ion-exchange resin, 3.6 g) was added and stirred for 2 h, after filtration, additional Amberlyst 15 (2 g) was added and stirred for another 2 h. After filtration, the solution was evaporated under reduced pressure, and the resulting off-white solid, H_2L_1 , was dried under vacuum overnight. Yield: 2.33 g, 9.21 mmol, 92%. Elemental analysis calcd (%) for $C_{11}H_{11}O_6N$ (253.21): C 52.18, H 4.38, N 5.53; found: C 52.83, H 3.99, N 5.21; 1H NMR (300 MHz, DMSO): $\delta = 9.18$ (s, 1H), 8.08 (d, 1H), 7.59 (d, 1H), 4.14 (m, 1H), 1.33 ppm (d, 3H); IR (KBr): 3436 (s), 1679 (m), 1635 (m), 1591 (s), 1513 (m), 1450 (w), 1417 (w), 1363 (m), 1251 (m), 1110 (m), 759 (m), 601 cm^{-1} (w).

Synthesis of $\{[\text{Tb}(\text{L}_1)_{1.5}(\text{H}_2\text{O})] \cdot 3\text{H}_2\text{O}\}_n$ (Tb-MOF)

Tb(NO₃)₃·6H₂O (31.0 mg, 0.07 mmol), H₂L (30.0 mg, 0.10 mmol), H₂O/CH₃CN (4/2 mL) were mixed in a Teflon-lined stainless steel vessel (25 mL). The mixture was heated under autogenous pressure at 120 °C for 72 h, and then cooled to RT. Colorless strip-shaped crystals (Tb-MOF) that were suitable for single-crystal X-ray analysis were obtained by filtration. The resulting crystals were washed with distilled water (yield: 89% based on terbium) and has a formula of $\{[\text{Tb}(\text{L}_1)_{1.5}(\text{H}_2\text{O})] \cdot 3\text{H}_2\text{O}\}_n$, which was derived from crystallographic data, elemental analysis (calcd (%): C 32.60, H 3.56, N 3.45; found: C 32.39, H 3.36, N 3.23), and TGA (Figure S3). IR (KBr): 3425 (s), 1652 (m), 1538 (s), 1461 (m), 1422 (s), 1380 (s), 1303 (m), 1269 (m), 1121 (w), 1084 (w), 1045 (w), 948 (w), 883 (w), 830 (w), 810 (w), 773 (m), 528 cm⁻¹ (m). The deprotection process took place during the synthesis of Tb-MOF: The acetyl group seems to be vital to this process, as replacing H₂L with H₂L₁ does not give crystals of Tb-MOF.

Luminescence sensing experiments

Tb-MOF (10 mg) was ground and immersed in water (1.5 mL), sonicated for 10 min to prepare the suspension, and then mixed with the aqueous solutions of M(NO₃)_x (0.02 mol L⁻¹, 1.5 mL) at room temperature (Mⁿ⁺ = Li⁺, Na⁺, K⁺, Mg²⁺, Ca²⁺, Sr²⁺, Ba²⁺, Cu²⁺, Co²⁺, Zn²⁺, Cd²⁺, Fe³⁺, Fe²⁺, Ni²⁺, or Al³⁺). The mixtures were then used for luminescent measurements.

Tb-MOF (10 mg) were ground and immersed in water (1.5 mL), sonicated for 10 min to prepare the suspension, and then mixed with the aqueous solutions of nitro explosives (0.02 mol L⁻¹ or saturated solution, 1.5 mL, NB, 1,3-DNB, 1,4-DNB, 2-NT, 2,4-DNT, 2,6-DNT, TNT, or TNP) at room temperature. The mixtures were then used for luminescent measurements.

Acknowledgements

This work was supported by the National Natural Science Foundation of China (No. 21371153) and the Program for Science & Technology Innovation Talents in Universities of Henan Province (13HASTIT008), the Key Scientific and Technological Project of Henan Province (132102210411) and Zhengzhou University.

Keywords: aqueous phase · metal-organic frameworks · microporous materials · multifunctional sensor · terbium

- [1] Special issues on metal-organic frameworks: a) *Chem. Soc. Rev.* **2009**, *38*, 1201–1508; b) *Chem. Rev.* **2012**, *112*, 673–1268; c) *Chem. Soc. Rev.* **2014**, *38*, 5415–6172.
- [2] a) S. Kitagawa, R. Kitaura, S. Noro, *Angew. Chem. Int. Ed.* **2004**, *43*, 2334–2375; *Angew. Chem.* **2004**, *116*, 2388–2430; b) A. Dhakshinamoorthy, H. Garcia, *Chem. Soc. Rev.* **2012**, *41*, 5262–5284; c) J.-S. Qin, D.-Y. Du, W.-L. Li, J.-P. Zhang, S.-L. Li, Z.-M. Su, X.-L. Wang, Q. Xu, K.-Z. Shao, Y.-Q. Lan, *Chem. Sci.* **2012**, *3*, 2114–2118; d) H. Wu, J. Yang, Z.-M. Su, S. R. Batten, J.-F. Ma, *J. Am. Chem. Soc.* **2011**, *133*, 11406–11409; e) J. Yang, B. Li, J.-F. Ma, Y.-Y. Liu, J.-P. Zhang, *Chem. Commun.* **2010**, *46*, 8383–8385.
- [3] a) B. V. Harbuzaru, A. Corma, F. Rey, J. L. Jorda, D. Ananias, L. D. Carlos, J. Rocha, *Angew. Chem. Int. Ed.* **2009**, *48*, 6476–6479; *Angew. Chem.* **2009**, *121*, 6598–6601; b) X. T. Rao, T. Song, J. K. Gao, Y. J. Cui, Y. Yang, C. D. Wu, B. L. Chen, G. D. Qian, *J. Am. Chem. Soc.* **2013**, *135*, 15559–15564; c) S. Dang, E. Ma, Z.-M. Sun, H. J. Zhang, *J. Mater. Chem.* **2012**, *22*, 16920–16926; d) H. Xu, X. T. Rao, J. K. Gao, J. C. Yu, Z. Q. Wang, Z. S. Dou, Y. J. Cui, Y. Yang, B. L. Chen, G. D. Qian, *Chem. Commun.* **2012**, *48*, 7377–7379; e) Y. Li, S. S. Zhang, D. T. Song, *Angew. Chem. Int. Ed.* **2013**, *52*, 710–713; *Angew. Chem.* **2013**, *125*, 738–741; f) P. Y. Wu, J. Wang, Y. M. Li, C. He, Z. Xie, C. Y. Duan, *Adv. Funct. Mater.* **2011**, *21*, 2788–2794.
- [4] a) J.-M. Zhou, W. Shi, H.-M. Li, H. Li, P. Cheng, *J. Phys. Chem. C* **2014**, *118*, 416–426; b) M. Zheng, H. Q. Tan, Z. G. Xie, L. G. Zhang, X. B. Jing, Z. C. Sun, *ACS Appl. Mater. Interfaces* **2013**, *5*, 1078–1083; c) J.-M. Zhou, W. Shi, N. Xu, P. Cheng, *Inorg. Chem.* **2013**, *52*, 8082–8090; d) M. C. Das, G. D. Qian, B. L. Chen, *Chem. Commun.* **2011**, *47*, 11715–11717.
- [5] a) S. Mohapatra, B. Rajeswaran, A. Chakraborty, A. Sundaresan, T. K. Maji, *Chem. Mater.* **2013**, *25*, 1673–1679; b) A. K. Chaudhari, S. S. Nagarkar, B. Joarder, S. K. Ghosh, *Cryst. Growth Des.* **2013**, *13*, 3716–3721; c) G.-Y. Wang, L.-L. Yang, Y. Li, H. Song, W.-J. Ruan, Z. Chang, X.-H. Bu, *Dalton Trans.* **2013**, *42*, 12865–12868; d) Y. Q. Xiao, Y. J. Cui, Q. Zheng, S. C. Xiang, G. D. Qian, B. L. Chen, *Chem. Commun.* **2010**, *46*, 5503–5505; e) W. T. Xu, Y. F. Zhou, D. C. Huang, M. Y. Su, K. Wang, M. C. Hong, *Inorg. Chem.* **2014**, *53*, 6497–6499; f) Q. Tang, S. X. Liu, Y. W. Liu, J. Miao, S. J. Li, L. Zhang, Z. Shi, Z. P. Zheng, *Inorg. Chem.* **2013**, *52*, 2799–2801.
- [6] a) A. Barba-Bon, A. M. Costero, S. Gil, *Chem. Commun.* **2012**, *48*, 3000–3002; b) J. L. Bricks, A. Kovalchuk, C. Trieflinger, M. Nofz, M. Buschel, A. I. Tolmachev, J. Daub, K. Rurack, *J. Am. Chem. Soc.* **2005**, *127*, 13522–13529.
- [7] a) V. K. Gupta, A. K. Jain, G. Maheshwari, *Talanta* **2007**, *72*, 1469–1473; b) T. P. Flaten, *Brain Res. Bull.* **2001**, *55*, 187–196.
- [8] R. Wang, X.-Y. Dong, H. Xu, R.-B. Pei, M.-L. Ma, S.-Q. Zang, H.-W. Hou, T. C. W. Mak, *Chem. Commun.* **2014**, *50*, 9153–9156.
- [9] a) Y. Zhou, H.-H. Chen, B. Yan, *J. Mater. Chem. A* **2014**, *2*, 13691–13697; b) J.-N. Hao, B. Yan, *J. Mater. Chem. A* **2014**, *2*, 18018–18025; c) J.-N. Hao, B. Yan, *J. Mater. Chem. C* **2014**, *2*, 6758–6764; d) Z. M. Hao, X. Z. Song, M. Zhu, X. Meng, S. N. Zhao, S. Q. Su, W. T. Yang, S. Y. Song, H. J. Zhang, *J. Mater. Chem. A* **2013**, *1*, 11043–11050; e) Z. Chen, Y. W. Sun, L. L. Zhang, D. Sun, F. L. Liu, Q. G. Meng, R. M. Wang, D. F. Sun, *Chem. Commun.* **2013**, *49*, 11557–11559.
- [10] a) Y. Salinas, R. Martinez-Manez, M. D. Marcos, F. Sancenon, A. M. Castero, M. Parra, S. Gil, *Chem. Soc. Rev.* **2012**, *41*, 1261–1296; b) M. E. Germain, M. J. Knapp, *Chem. Soc. Rev.* **2009**, *38*, 2543–2555.
- [11] a) Y. J. Cui, Y. F. Yue, G. D. Qian, B. L. Chen, *Chem. Rev.* **2012**, *112*, 1126–1162; b) Z. J. Zhang, S. C. Xiang, X. T. Rao, Q. Zheng, F. R. Fronczek, G. D. Qian, B. L. Chen, *Chem. Commun.* **2010**, *46*, 7205–7207; c) H. Xu, F. Liu, Y. J. Cui, B. L. Chen, G. D. Qian, *Chem. Commun.* **2011**, *47*, 3153–3155; d) B. Gole, A. K. Bar, P. S. Mukherjee, *Chem. Eur. J.* **2014**, *20*, 2276–2291.
- [12] a) S. S. Nagarkar, B. Joarder, A. K. Chaudhari, S. Mukherjee, S. K. Ghosh, *Angew. Chem. Int. Ed.* **2013**, *52*, 2881–2885; *Angew. Chem.* **2013**, *125*, 2953–2957; b) S. Das, P. K. Bharadwaj, *Inorg. Chem.* **2006**, *45*, 5257–5259; c) C. Wang, W. B. Lin, *J. Am. Chem. Soc.* **2011**, *133*, 4232–4235; d) C. Y. Zhang, Y. K. Che, Z. X. Zhang, X. M. Yang, L. Zang, *Chem. Commun.* **2011**, *47*, 2336–2338; e) H. L. Jiang, Y. Tatsu, Z. H. Lu, Q. Xu, *J. Am. Chem. Soc.* **2010**, *132*, 5586–5587.
- [13] a) D. Banerjee, Z. C. Hu, J. Li, *Dalton Trans.* **2014**, *43*, 10668–10685; b) S.-N. Zhao, X.-Z. Song, M. Zhu, X. Meng, L.-L. Wu, S.-Y. Song, C. Wang, H.-J. Zhang, *RSC Adv.* **2015**, *5*, 93–98; c) A. Lan, K. Li, H. Wu, D. H. Olson, T. J. Emge, W. Ki, M. C. Hong, J. Li, *Angew. Chem. Int. Ed.* **2009**, *48*, 2334–2338; *Angew. Chem.* **2009**, *121*, 2370–2374.
- [14] G. He, H. N. Peng, T. H. Liu, M. N. Yang, Y. Zhang, Y. Fang, *J. Mater. Chem.* **2009**, *19*, 7347–7353.
- [15] a) B. Joarder, A. V. Desai, P. Samanta, S. Mukherjee, S. K. Ghosh, *Chem. Eur. J.* **2015**, *21*, 965–969; b) S. S. Nagarkar, A. V. Desai, S. K. Ghosh, *Chem. Commun.* **2014**, *50*, 8915–8918; c) W. Xie, S.-R. Zhang, D.-Y. Du, J.-S. Qin, S.-J. Bao, J. Li, Z.-M. Su, W.-W. He, Q. Fu, Y.-Q. Lan, *Inorg. Chem.* **2015**, *54*, 3290–3296.
- [16] B. W. Xu, X. F. Wu, H. B. Li, H. Tong, L. X. Wang, *Macromolecules* **2011**, *44*, 5089–5092.
- [17] a) T. M. Reineke, M. Eddaoudi, M. Fehr, D. Kelley, O. M. Yaghi, *J. Am. Chem. Soc.* **1999**, *121*, 1651–1657; b) W. J. Rieter, K. M. L. Taylor, H. Y. An, W. L. Lin, W. B. Lin, *J. Am. Chem. Soc.* **2006**, *128*, 9024–9025.
- [18] CCDC 1053509 (Tb-MOF) contains the supplementary crystallographic data for this paper. These data are provided free of charge by The Cambridge Crystallographic Data Centre.
- [19] a) X.-Z. Song, S.-Y. Song, S.-N. Zhao, Z.-M. Hao, M. Zhu, X. Meng, L.-L. Wu, H.-J. Zhang, *Adv. Funct. Mater.* **2014**, *24*, 4034–4041; b) Y. B. He, S. C. Xiang, Z. J. Zhang, S. S. Xiong, F. R. Fronczek, R. Krishna, M. O'Keefe, B. L. Chen, *Chem. Commun.* **2012**, *48*, 10856–10858; c) N. L. Rosi, J.

- Kim, M. Eddaoudi, B. L. Chen, M. O'Keeffe, O. M. Yaghi, *J. Am. Chem. Soc.* **2005**, *127*, 1504–1518.
- [20] A. L. Spek, *J. Appl. Crystallogr.* **2003**, *36*, 7–13.
- [21] a) V. A. Blatov, M. V. Peaskov, *Acta Crystallogr. Sect. B* **2006**, *62*, 457–466; b) V. A. Blatov, A. P. Shevchenko, V. N. Serezhkin, *J. Appl. Crystallogr.* **2000**, *33*, 1193.
- [22] B. L. Chen, L. B. Wang, Y. Q. Xiao, F. R. Fronczek, M. Xue, Y. J. Cui, G. D. Qian, *Angew. Chem. Int. Ed.* **2009**, *48*, 500–503; *Angew. Chem.* **2009**, *121*, 508–511.
- [23] C. X. Yang, H. B. Ren, X. P. Yan, *Anal. Chem.* **2013**, *85*, 7441–7446.
- [24] a) J. Z. Liu, Y. C. Zhong, P. Lu, Y. N. Hong, J. W. Y. Lam, M. Faisal, Y. Yu, K. S. Wong, B. Z. Tang, *Polym. Chem.* **2010**, *1*, 426–429; b) X.-H. Zhou, L. Li, H.-H. Li, A. Li, T. Yang, W. Huang, *Dalton Trans.* **2013**, *42*, 12403–12409.
- [25] W. Luo, Y. Zhu, J. Zhang, J. He, Z. Chi, P. W. Miller, L. Chena, C. Y. Sua, *Chem. Commun.* **2014**, *50*, 11942–11945.
- [26] a) K. N. Slessor, G. G. S. King, D. R. Miller, M. L. Winston, H. Cutforth, *J. Chem. Ecol.* **1985**, *11*, 1659–1667; b) R. Hulst, N. K. de Vries, B. L. Feringa, *Tetrahedron* **1994**, *50*, 11721–11728.

Received: March 24, 2015

Published online on September 10, 2015